Lamb, GP, Tanaka, M and Kobayashi, S

Transient Survey Rates for Orphan Afterglows from Compact Merger Jets

Article

Lamb, GP, Tanaka, M and Kobayashi, S (2018) Transient Survey Rates for Orphan Afterglows from Compact Merger Jets. Monthly Notices of the Royal Astronomical Society, 476 (4). pp. 4435-4441. ISSN 0035-8711

Monthly Notices of the ROYAL ASTRONOMICAL SOCIETY

MNRAS **476,** 4435–4441 (2018) doi:10.1093/mnras/sty484
Advance Access publication 2018 February 22

Transient survey rates for orphan afterglows from compact merger jets

Gavin P. Lamb,[1,3]★ Masaomi Tanaka[2] and Shiho Kobayashi[1]

[1]*Astrophysics Research Institute, LJMU, IC2, Liverpool Science Park, 146 Brownlow Hill, Liverpool L3 5RF, UK*
[2]*National Astronomical Observatory of Japan (NAOJ), Tokyo, Japan*
[3]*Department of Physics and Astronomy, University of Leicester, University Road, Leicester, LE1 7RH, UK*

Accepted 2018 February 18. Received 2018 February 5; in original form 2017 December 1

ABSTRACT

Orphan afterglows from short γ-ray bursts (GRBs) are potential candidates for electromagnetic (EM) counterpart searches to gravitational wave (GW) detected neutron star or neutron star black hole mergers. Various jet dynamical and structure models have been proposed that can be tested by the detection of a large sample of GW–EM counterparts. We make predictions for the expected rate of optical transients from these jet models for future survey telescopes, without a GW or GRB trigger. A sample of merger jets is generated in the redshift limits $0 \leq z \leq 3.0$, and the expected peak r-band flux and time-scale above the Large Synoptic Survey Telescope (LSST) or Zwicky Transient Factory (ZTF) detection threshold, $m_{\rm r} = 24.5$ and 20.4, respectively, is calculated. General all-sky rates are shown for $m_{\rm r} \leq 26.0$ and $m_{\rm r} \leq 21.0$. The detected orphan and GRB afterglow rate depends on jet model, typically $16 \lesssim R \lesssim 76\,{\rm yr}^{-1}$ for the LSST, and $2 \lesssim R \lesssim 8\,{\rm yr}^{-1}$ for ZTF. An excess in the rate of orphan afterglows for a survey to a depth of $m_{\rm r} \leq 26$ would indicate that merger jets have a dominant low-Lorentz factor population, or the jets exhibit intrinsic jet structure. Careful filtering of transients is required to successfully identify orphan afterglows from either short- or long-GRB progenitors.

Key words: gamma-ray burst: general.

1 INTRODUCTION

The most promising candidate for the progenitor of short γ-ray bursts (GRBs) is the merger of a binary neutron star (NS) system or a NS black hole (BH) system (e.g. Eichler et al. 1989; Narayan, Paczynski & Piran 1992; Mochkovitch et al. 1993; Bogomazov, Lipunov & Tutukov 2007; Nakar 2007; Berger 2014). Such systems are candidate targets for gravitational wave (GW) detectors, and as such there has been a focus on potential electromagnetic (EM) counterparts to such mergers (Nissanke, Kasliwal & Georgieva 2013). Amongst the counterparts are the isotropic macro-/kilo-nova (e.g. Li & Paczyński 1998; Barnes & Kasen 2013; Tanaka & Hotokezaka 2013; Piran, Nakar & Rosswog 2013; Metzger & Fernández 2014; Tanaka et al. 2014, 2017, 2018; Barnes et al. 2016; Tanaka 2016; Metzger 2017), radio counterparts (e.g. Nakar & Piran 2011; Kyutoku, Ioka & Shibata 2014; Margalit & Piran 2015; Hotokezaka & Piran 2015; Hotokezaka et al. 2016), wide-angle cocoon emission (Lazzati et al. 2017; Kisaka et al. 2017; Nakar & Piran 2017; Gottlieb, Nakar & Piran 2018), resonant shattering, merger-shock, or precursor flares (Tsang et al. 2012; Kyutoku et al. 2014; Metzger & Zivancev 2016), GRBs (e.g. Coward et al. 2014; Ghirlanda et al. 2016; Kathirgamaraju, Barniol Duran & Giannios 2018; Jin et al. 2017), failed GRBs (fGRB) (Dermer, Chiang & Mitman 2000; Huang, Dai & Lu 2002; Nakar & Piran 2003; Rhoads 2003; Lamb & Kobayashi 2016, 2017), and off-axis orphan afterglows (e.g. Granot et al. 2002; Rossi, Lazzati & Rees 2002; Zou, Wu & Dai 2007; Zhang 2013; Lazzati et al. 2017; Sun, Zhang & Gao 2017). Some of these counterparts make promising potential transients for the next generation of optical survey telescopes, e.g. Large Synoptic Survey Telescope (LSST) (LSST Science Collaboration et al. 2009), and Zwicky Transient Facility (ZTF) (e.g. Bellm 2014; Bellm & Kulkarni 2017) .

Here, we make predictions for transient rates in blind surveys (i.e. without a GW or γ-ray trigger), for orphan afterglows from short-GRB jets and transients based on the expected excess as a result of low-Lorentz factor fGRB jets (Lamb & Kobayashi 2016) and/or jets with extended wide structure (e.g. Jin et al. 2017; Kathirgamaraju et al. 2018; Lamb & Kobayashi 2017; Xiao et al. 2017). Different jet structures predict different emission properties, especially for off-axis viewing angles. Therefore, the detection rate of orphan afterglows will give an important constraint on the structure and dynamics of the jets. We consider only the transients from the afterglow due to the jet–ISM (interstellar medium) interaction; such transients will be associated with all jetted short-GRB progenitor models and the jet afterglow, orphan or otherwise, will have a non-thermal spectrum. Where short GRBs are exclusively due to NS/BH–NS mergers, then additional transients will be associated; most notably a macro-/kilo-nova that will have a red/infrared frequency peak brightness that depends on the viewing

★ E-mail: gpl6@le.ac.uk

angle, and an earlier blue/ultraviolet peak that will be apparent depending on the system inclination. Macro-/kilo-nova emission will have a thermal spectrum and a very rapid decline after the peak.

In Section 2 we describe the merger jet parameters and models used, and in Section 3 we describe the method for generating the cosmological population of merger jets. The results are described in Section 4 and discussed in Section 5. Concluding remarks are made in Section 6.

2 MERGER JET MODELS

We assume that the dominant progenitor for the short-GRB population is relativistic jets from mergers (Levan et al. 2016). From the observed energetics of short GRBs a luminosity function can be determined (e.g. Wanderman & Piran 2015; Sun, Zhang & Li 2015; Ghirlanda et al. 2016; Zhang & Wang 2018).

We generate seven populations of merger jets where we use a Wanderman & Piran (2015) redshift and luminosity function. Four populations have homogeneous jet structure models:

(i–iii) WP15$_{6/16/26}$: With a coasting phase bulk Lorentz factor $\Gamma = 100$ and a jet half-opening angle[1] of $\theta_{\rm j} = 16 \pm 10^{\circ}$ (Fong et al. 2015). For population (i) $\theta_{\rm j} = 6^{\circ}$, (ii) $\theta_{\rm j} = 16^{\circ}$, and (iii) $\theta_{\rm j} = 26^{\circ}$.

(iv) LK16: With a bulk Lorentz factor distribution for the population defined as $N(\Gamma) \propto \Gamma^{-2}$ with a range $2 \le \Gamma \le 10^{3}$ (Lamb & Kobayashi 2016). We assume each jet has a half-opening angle $\theta_{\rm j} = 16^{\circ}$.

The final three jet populations use parameters that are described by the structured jet models in Lamb & Kobayashi (2017). These jets have a core angle $\theta_{\rm c} = 6^{\circ}$ and a wider jet component to $\theta_{\rm j} = 25^{\circ}$ in each case. For the structured jets, the luminosity function is used to determine the power within the jet core.

(v) LK17t: Two-component jets where the wider component $\theta_{\rm c} < \theta \le \theta_{\rm j}$ has energy and Lorentz factor at 5 per cent the core value.

(vi) LK17p: Power-law jets where the energy and Lorentz factor between the core and jet edge scale with angle from the core using a negative index power law, $\propto (\theta/\theta_c)^{-2}$.

(vii) LK17g: Gaussian jets where the energy and Lorentz factor follow a Gaussian function with angle to the jet edge, $\propto e^{-\theta^2/2\theta_{\rm c}^2}$.

The existence of a jet edge for the structured jet models is motivated by relativistic magnetohydrodynamic simulations of NS mergers (e.g. Rezzolla et al. 2011; Dionysopoulou, Alic & Rezzolla 2015)

3 METHOD

We assume the short-GRB rate[2] and luminosity function given in Wanderman & Piran (2015); note the event rate for this distribution varies with redshift, peaking at $z = 0.9$, and rapidly declines with increasing redshift ($R_{\rm GRB} = 45\,{\rm e}^{(z-0.9)/0.39}$ Gpc^{-3} yr^{-1}, where $z \le 0.9$, and $R_{\rm GRB} = 45\,{\rm e}^{-(z-0.9)/0.26}$ for $z > 0.9$). At redshifts below the peak, the event rate is consistent with that found by D'Avanzo et al. (2014) and Sun et al. (2015). The luminosity function follows a broken power law with the limits $5 \times 10^{49} \le L_{\gamma} \le 10^{53}$ erg s^{-1} and a brake at 2×10^{52} erg s^{-1}; at luminosities below the brake the power-law index is -1, and above the brake the index is -2. The luminosity function is defined with an interval $d\log L_{\gamma}$. Note that we do not consider low-luminosity short GRBs, i.e. $L_{\gamma} < 5 \times 10^{49}$ erg s^{-1}. The origin of low-luminosity short GRBs is not known, the low-luminosity population could represent an extension of the usual short-GRB luminosity function to lower powers or a distinct population of low-luminosity short GRBs (e.g. Siellez et al. 2016). The afterglows from a population of low-luminosity GRBs would be intrinsically very faint and the redshift distribution of the observable sample limited to 'local' luminosity distances.

Using the short-GRB rate (Gpc^{-3} yr^{-1}) and luminosity function, a correlation for isotropic equivalent energy and νF_{ν} spectral peak energy $E_{\rm p}$ in Tsutsui et al. (2013), and assuming a spectral index $\alpha = 0.5$ and $\beta = 2.25$ (Gruber et al. 2014) with a broken power law, we find the minimum γ-ray luminosity for a detectable short GRB and the rate at a given redshift. We assume a detection if the number of photons in the energy band 15–150 keV is $\ge$0.3 ph cm^{-2} s^{-1} (Band 2006). Using the minimum observable luminosity and the short-GRB rate with redshift, the all-sky number of detectable short GRBs is $\sim$71 yr^{-1}. *Swift*/BAT detects $\sim$10 yr^{-1}, however as noted by Bromberg et al. (2013), the *Swift*/BAT short-GRB sample is contaminated by non-merger (collapsar) short duration GRBs, the fraction of merger short GRBs is $\sim$60 per cent . Using a detection rate of $\sim$6 yr^{-1}, the effective field of view for *Swift*/BAT is $\sim$1.06 sr, this is less than the Burst Alert Telescope (BAT) partially coded field of view $\sim$1.4 sr (Baumgartner et al. 2013). The *Swift*/BAT duty cycle, the sensitivity of the partially coded field of view, or the exact fraction of merger short GRBs may explain this discrepancy. The all-sky rate for short GRBs is used to normalize the Monte Carlo merger jet samples.

For each model (i–vii), 10^5 merger-jets are generated. Each jet has a random isotropically distributed inclination i to the line of sight and a random redshift z using the short-GRB redshift distribution. The jet energetics and bulk Lorentz factor depend on the model parameters. The prompt emission is highly beamed and only detectable for typical cosmological distances and γ-ray energies from jets inclined within the jet half-opening angle. The γ-ray photon flux at the detector for a jet inclined within the half-opening angle is calculated considering the jet luminosity. A correlation between the γ-ray luminosity and spectral peak energy for short GRBs is used to determine $E_{\rm p}$ (e.g. Yonetoku et al. 2004; Ghirlanda et al. 2009; Zhang et al. 2012; Tsutsui et al. 2013). We use the same GRB detection criteria as that used to estimate the all-sky *Swift*/BAT short-GRB rate.

Using the fireball model (Piran 1999) and an assumed γ-ray efficiency η for the prompt emission, the isotropic equivalent blast energy can be found from the γ-ray luminosity L_{γ} and time-scale T_{90}. The jet kinetic energy $E_{\rm k} = L_{\gamma}T_{90}(1/\eta - 1)$ is dissipated in shocks that form as the jet decelerates in the ambient medium giving rise to an afterglow. The temporal evolution and peak afterglow flux of a GRB follows Sari, Piran & Narayan (1998); Sari, Piran & Halpern (1999), where the peak flux is $F_{\rm p} \propto n^{1/2}\varepsilon_{\rm B}^{1/2}E_{\rm k}D^{-2}$, here n is the ambient number density, ε_B is the microphysical magnetic parameter, and D is the luminosity distance.

For an off-axis observer, at an inclination greater than the jet half-opening angle $\theta_{\rm j}$, the observed flux is reduced by relativistic effects. The flux at a given observer frequency ν becomes $F_{\nu}(i, t) = a^3 F_{\nu/a}(0, at)$, where $a = \delta(i)/\delta(i=0)$ and $\delta = [\Gamma(1-\beta\cos i)]^{-1}$ is the relativistic Doppler factor; Γ is the bulk Lorentz factor, and

[1] Note that Ghirlanda et al. (2016) found this redshift distribution to indicate jet half-opening angles in the range $7^{\circ} \le \theta_{\rm j} \le 14^{\circ}$, we use the wider angle and range to include the widest observations $\theta_{\rm j} \gtrsim 25^{\circ}$.

[2] Cosmological parameters $H_0 = 70$, $\Omega_M = 0.3$, and $\Omega_{\Lambda} = 0.7$ are used throughout.

Table 1. The number of afterglow transients from a given merger jet model that are brighter than a limiting *r*-band magnitude. All models use the redshift and luminosity function from Wanderman & Piran (2015). The GRB population in each sample is normalized to an all sky rate of *Swift*/BAT detectable short GRBs of $\sim$71 yr^{-1}. The first value in each column is for orphan afterglows only, the values in square brackets are for GRB and orphan afterglows combined. The all-sky rates less than a given magnitude have an associated uncertainty of $\sim\pm0.7$ deg^{-2} yr^{-1}. The LSST and ZTF detection rate is based on the mean time-scale a transient is brighter than the telescope threshold.

	Model	≤26 $\times 10^{-3}$ deg^{-2} yr^{-1}	≤24.5 $\times 10^{-3}$ deg^{-2} yr^{-1}	≤21 $\times 10^{-3}$ deg^{-2} yr^{-1}	≤20.4 $\times 10^{-3}$ deg^{-2} yr^{-1}	$\langle T_{\rm LSST}\rangle$ days	LSST yr^{-1}	$\langle T_{\rm ZTF}\rangle$ days	ZTF yr^{-1}
(i)	WP15$_6$	32.2 [33.6]	25.3 [26.7]	3.6 [5.0]	1.4 [2.8]	0.16 [0.20]	13.4 [17.6]	0.02 [0.03]	0.6 [1.9]
(ii)	WP15$_{16}$	20.2 [22.9]	18.5 [21.1]	2.3 [5.0]	0.8 [3.1]	0.12 [0.27]	7.3 [18.8]	0.03 [0.06]	0.5 [4.2]
(iii)	WP15$_{26}$	15.7 [17.5]	15.0 [16.7]	3.5 [5.2]	1.6 [3.3]	0.11 [0.34]	5.4 [18.7]	0.02 [0.07]	0.7 [5.2]
(iv)	LK16	60.0 [62.0]	39.2 [41.2]	3.7 [5.7]	1.8 [3.7]	0.54 [0.56]	70.0 [76.1]	0.09 [0.07]	3.6 [5.8]
(v)	LK17t	27.6 [29.3]	21.8 [23.5]	2.5 [4.2]	0.9 [2.5]	0.18 [0.30]	12.8 [23.2]	0.03 [0.11]	0.6 [6.2]
(vi)	LK17p	43.6 [45.4]	29.3 [31.1]	3.3 [5.0]	1.3 [2.9]	0.11 [0.25]	10.6 [25.7]	0.03 [0.12]	0.9 [7.8]
(vii)	LK17g	50.3 [51.5]	34.4 [35.5]	2.8 [4.0]	1.3 [2.5]	0.08 [0.14]	9.1 [16.4]	0.03 [0.07]	0.9 [3.9]

β is the jet velocity relative to the speed of light (Granot et al. 2002). Note that this relation is valid for a point source only and that for a jet with a defined opening angle the relativistic beaming factor for the flux is $\sim a^2$ for $i \lesssim 2\theta_{\rm j}$, and the angle used to calculate the relativistic Doppler factor is $i - \theta_{\rm j}$ where $i > \theta_{\rm j}$ (Kumar & Panaitescu 2000; Ioka & Nakamura 2001).

For all jets we use the method in Lamb & Kobayashi (2017), with the relevant jet structure model to generate on-/off-axis afterglows for the population of jets. The ambient density is assumed to be $n = 0.1$ cm^{-3}, microphysical parameter $\varepsilon_{\rm e} = 0.1$, $\varepsilon_{\rm B} = 0.01$, particle distribution index $p = 2.5$, and γ-ray radiation efficiency $\eta = 0.1$. For each population, the normalized number of *Swift*/BAT GRBs and orphan afterglows are counted.

Using the distribution of peak afterglows from a given model and a transient survey telescope's per night coverage, the number of transients with or without a GRB that have an optical counterpart brighter than the survey's detection threshold can be found. For transients in our sample that are brighter than the LSST(ZTF) survey threshold, *r*-band magnitude $\sim$24.5(20.4), we determine the number that are brighter than this limit for $\geq$4(1) d. This ensures a minimum of two detections within the proposed cadence. For LSST, we use a survey rate of $\sim$3300 deg^2 night^{-1}, covering $\sim$0.08 of the whole sky per night; for ZTF the survey rate is $\sim$3760 deg^2 h^{-1} where the average night is 8 h 40 m (Bellm 2014). ZTF will cover $\sim$0.09 of the whole sky per hour, and considering the observable fraction of the sky per night, will cover $\sim$22,500 deg^2 night^{-1} or $\sim$0.55 of the whole sky per night with a 1 d cadence.

4 RESULTS

The rate of afterglow transients for each model is shown in Table 1. The various models are described in Section 2. For LK17t, LK17p, and LK17g (v–vii), the opening angle at which a GRB is detectable depends on the distance, luminosity, and inclination of the source. For the WP15 (i–iii) and LK16 (iv) models, a GRB is typically only detectable for inclinations that are less than the jet half-opening angle, $i \lesssim \theta_{\rm j}$. [3]

Fig. 1 shows the number of afterglow transients per square degree per year brighter than a given *r*-band magnitude from merger jets. Each model is indicated by a different colour and line style as described in the figure caption. Each distribution is for both GRB and orphan afterglows (the value in square brackets in Table 1).

[3] Merger jets at very low redshift or with very high energy may be detectable at γ-ray energies for inclinations just outside of the jet half-opening angle.

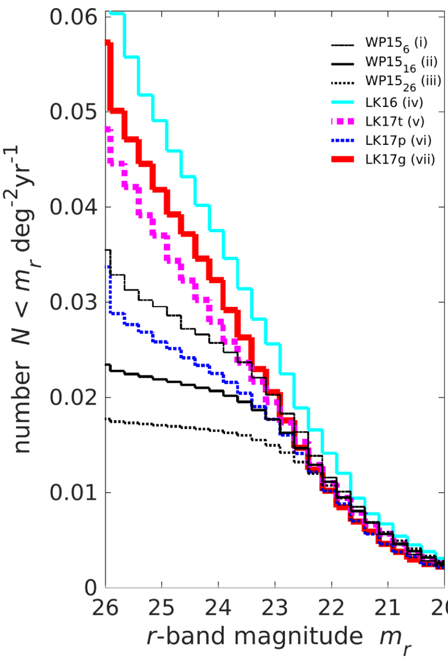

Figure 1. The number of afterglows (deg^{-2} yr^{-1}) brighter than a given magnitude for each jet model in $\Delta m_{\rm r} = 0.25$ magnitude bins. The homogeneous jet models (i–iii) with a half-opening angle $\theta_{\rm j} = 6°$ with a thin black dashed-dotted line, $\theta_{\rm j} = 16°$ are a black solid line, and $\theta_{\rm j} = 26°$ with a thin black dotted line. The afterglows from the low-Lorentz factor jets model (iv) are shown with a medium thickness solid cyan line. The structured jet models (v–vii) are shown with a thin blue dotted line for the two-component model, a thick pink dotted line for the power-law structured jets, and a thick red solid line for the Gaussian structured jets.

We assume a fixed ambient density for all events of $n = 0.1$ cm^{-3}. However, the density for short GRB environments has a broad range and the peak flux depends on the ambient density as $\propto n^{1/2}$. As 40–80 per cent of the short GRB population, where $\varepsilon_{\rm B} = 0.01$, has $n > 0.1$ cm^{-3} (Fong et al. 2015), then considering the full ambient density range, the presented results are not significantly changed.

The homogeneous jet models with a fixed initial Lorentz factor WP15 (i–iii) produce detectable GRBs, where the detector has our parameters and sensitivity, for $\sim 9 \pm 1$ per cent of merger-jets that are inclined within the jet half-opening angle. For homogeneous jets the typical inclination for on-axis, $i < \theta_{\rm j}$, orphan afterglows and/or GRB detected systems is $\sim 2\theta_{\rm j}/3$; for off-axis, $i > \theta_{\rm j}$, the orphan afterglow is typically observed at an angular separation of $\sim\theta_j + 1.1^\circ$, where the limiting magnitude is ≤ 26.

The typical redshift for a detected GRB with our detection criteria and parameters, for all of the jet models, is $\langle z\rangle = 0.50 \pm 0.07$. The uncertainty represents the different model mean values. The measured mean redshift value for the population of *Swift*/BAT short GRBs with redshift is $\langle z\rangle = 0.49$ (Berger 2014). For the orphan afterglow populations the typical redshift is sensitive to the limiting magnitude. Where the afterglow peaks ≤ 26 and for the LSST sample where the peak ≤ 24.5 then $\langle z\rangle = 0.90 \pm 0.05$; for the limit of ≤ 21 and the ZTF sample with ≤ 20.4 then $\langle z\rangle = 0.80 \pm 0.05$ and $\langle z\rangle = 0.70 \pm 0.05$, respectively. For the peak magnitude limited samples, ≤ 26 and ≤ 24.5, the mean redshift coincides with the peak of the redshift distribution. For a rate that peaks at a higher redshift, the mean for the peak magnitude ≤ 26 and ≤ 24.5 transients is higher. Where a redshift distribution peaks at $z \sim 1.5$, the mean is $\langle z\rangle = 1.75$ and $\langle z\rangle = 1.46$, respectively. A significant fraction of all orphan afterglows in our sample are viewed on-axis, i.e. within the jet half-opening angle. The prompt GRB can be undetected despite being favourably inclined due to the dynamics of the jet model, the detector sensitivity, γ-ray efficiency, and/or distance. The orphan afterglow in such a case will be phenomenologically the same as a regular GRB afterglow (e.g. Cenko et al. 2013).

If detections are limited to two points brighter than the limiting magnitude in the given cadence of a survey telescope, then for LSST using a cadence of 4 d the number of transients brighter than magnitude 24.5 and the number for ZTF with a 1 d cadence but limiting magnitude of 20.4 is small in all cases. For the LSST sample, with or without a GRB, the fraction of transients brighter than the threshold for the 4 d cadence considered is $\sim 0.04 \pm 0.01$. For ZTF, this fraction is $\lesssim 0.06$ for a 1 d cadence. These fractions are insensitive to the jet model.

5 DISCUSSION

We have generated a Monte Carlo distribution of merger jets for each of the jet models considered: a population of homogeneous jets with a jet half-opening angle of 6°, 16°, or 26°; a population of merger jets that have an independent Lorentz factor following a negative index power-law distribution; and three structured jet models, all with a core value of 6° and a jet edge at 25°. The merger jets follow a Wanderman & Piran (2015) redshift distribution for merger (non-collapsar) short GRBs and have a random isotropic inclination. For each event the γ-ray photon flux at the detector in the energy band 15–150 keV is determined, if the flux is greater than the threshold value then a GRB is detectable. Each population of merger-jets is normalized by the all-sky rate of *Swift*/BAT detectable short GRBs.

The fraction of on-axis events $i < \theta_j$ will follow the probability distribution for a randomly oriented bipolar jet system with the jet half-opening angle θ_j, i.e. $1 - \cos\theta_j \sim \theta_j^2/2$. Not all on-axis events will produce a detectable GRB or afterglows above the detection threshold. For all models considered this is due to a combination of luminosity, distance to a merger, and spectral peak energy. For the LK16 and structured jet models, the fGRB fraction is higher due to suppression of the prompt emission in the low-Γ/energy jet/components.

Forward shock afterglow transients from short GRBs, on-axis fGRBs, and off-axis orphan afterglows are detectable by both the LSST and ZTF. The rate for both LSST and ZTF detectable transients depends on the nature of the jets in a population of mergers. Where the jet Lorentz factor varies from jet to jet, only a small fraction of the merger jets, when viewed on-axis, will produce a detectable GRB (e.g. Lamb & Kobayashi 2016). Afterglows are typically fainter for a population of low-Γ fGRBs, this is due to the later deceleration time for the jet where $t_{\rm dec} \propto \Gamma^{-8/3}$, and the lower characteristic synchrotron frequency, $\nu_{\rm m} \propto \Gamma^4$, meaning the optical peak flux is lower than the maximum synchrotron flux as $\nu_{\rm obs} > \nu_{\rm m}$ at the peak time. This is reflected in the orphan afterglow rate being $\sim$2–3$\times$ larger for LK16 model (iv) than for $\mathrm{WP15}_{16}$ model (ii), where $\Gamma = 100$ for all events.

For jets with structure, the orphan afterglows are typically brighter than the orphan afterglows for a population of homogeneous jets (Lamb & Kobayashi 2017). Structured jets have higher latitude jet components with a low-Γ that can suppress a GRB for an observer at these inclinations, thus structured jets can produce a larger fraction of orphan afterglows where the inclination is less than the jet half-opening angle. These orphans are typically brighter than a homogeneous jet described by the γ-ray bright region of a structured jet. However, for the two-component jet LK17t model (v) it is clear from Fig. 1 that the rate of transients is $\sim$80 per cent that of the rate for a homogeneous jet population with $\theta_j = 6^\circ$, $\mathrm{WP15}_6$ model (iii). The two-component model will typically have a γ-ray bright core, $\theta_c = 6^\circ$, and an extended 'sheath' that generally fails to produce detectable GRBs. For model (iii), θ_j is equivalent to the core size in the two-component model. Due to the two-component models extended structure, GRBs are observable at $i > \theta_c$ in jets where the core luminosity is very high or the merger is nearby. Therefore, the fraction of GRBs from this model is larger than that for the 6° homogeneous jet model and thus when the distributions are normalized the total number of mergers is smaller.

To consider the fraction of afterglows detected by blind sky surveys, the typical time period for which a transient is brighter than the limiting magnitude is determined. For the LSST(ZTF) limit of 24.5(20.4), the typical time-scale is shown in Table 1. The product of the all-sky rate ($\mathrm{deg}^{-2}\,\mathrm{yr}^{-1}$), the per night survey field of view ($\mathrm{deg}^2\ \mathrm{d}^{-1}$), and the typical time-scale for a transient (day) give the expected rate of detectable transients for a survey. For LSST, the chance of detecting an orphan afterglow from a merger jet is reasonable, $5 \lesssim R_{\rm OA} \lesssim 70\,\mathrm{yr}^{-1}$, depending on the jet model. If we consider both orphan and GRB afterglows the rate increases, $16 \lesssim R_{\rm AG} \lesssim 76\,\mathrm{yr}^{-1}$. For ZTF the rate of detected orphan afterglows from merger jets is low, $0.5 \lesssim R_{\rm OA} \lesssim 3.6\,\mathrm{yr}^{-1}$. The combined orphan and GRB afterglow rate is more promising, $2 \lesssim R_{\rm AG} \lesssim 8\,\mathrm{yr}^{-1}$. However, in each case, the afterglow transients are rarely brighter than the detection threshold for longer than the cadence.

The differentiation between merger-jet origin orphan afterglows and collapsar or long-GRB jet orphans will be difficult. Ghirlanda et al. (2015) predicts a rate of $R_{\rm OA} \sim 50\,\mathrm{yr}^{-1}$ for the LSST from long-GRB jets. For faint transients, the peak flux may not be brighter than the host galaxy, magnitude $\sim$24–27 (Berger 2014) . In such a case, the detection of a transient will depend on the survey angular resolution and the image subtraction technique. However, short GRBs can be hostless or have typically large offsets from the bright core or star-forming regions, but in such cases the ambient density is low and the peak flux will be fainter. Long GRBs are typically associated with star-forming galaxies and regions (e.g. Bloom et al. 1998; Djorgovski et al. 1998; Fruchter et al. 2006), making faint orphan transients from long-GRB jets more difficult to detect. Short GRB host galaxies systematically have an older stellar population, have a lower star-formation rate, and a higher metallicity than the host galaxies for long GRBs (Berger 2014). Note however that short GRB host galaxies can be both early- and late-type galaxies.

Additionally, simulations performed by O'Shaughnessy et al. (2017) suggest that short GRB merger progenitor systems are over-produced by dwarf galaxies; these galaxies are typically faint with surface brightness $-14 \lesssim M_{\rm B} \lesssim -10$ (Sabatini, Roberts & Davies 2003), approximately 28–32 mag at $z = 0.5$. Alternatively, by considering the natal kick velocities of NS–NS systems, the fraction of hostless short GRBs, and the dark matter potential well of galaxies, Behroozi, Ramirez-Ruiz & Fryer (2014) found that short GRBs are expected to be associated with galaxies that have a stellar mass $(5 \pm 3) \times 10^{10}$ $M_{\odot}$. The differences in the host galaxy and location within the host galaxy may be used to distinguish between the progenitor of GRB-less transients.

The predicted low detection rates for merger jet transients can result in confusion not only between a collapsar jet and merger jet origin but also, and perhaps dominantly, from other astrophysical transients. Flares from active galactic nuclei (AGN), tidal disruption events (TDEs), and rapidly evolving faint supernovae (SNe) are amongst the confusion sources for fast and faint extragalactic transients. For these events, the location within the host galaxy can help distinguish the origin, where AGN and TDEs are expected to be located within the core of a galaxy. Spectroscopy, or colour evolution that can trace the underlying spectrum, is required to reliably distinguish between a non-thermal jet afterglow transient and a SNe or SN-like transients. However, a thermal transient that either precedes or follows the non-thermal jet transient will indicate a merger origin, see discussion below.

By considering the other associated transients for a NS/BH–NS merger, i.e. resonant shattering flares or impact flares for NS mergers (Tsang et al. 2012; Kyutoku et al. 2014) or SNe for long GRBs, the origin of the orphan afterglow may be additionally constrained for nearby events. With the development of next generation GW detectors, e.g. the Einstein Telescope (ET) (Punturo et al. 2010), the volume within which a NS/BH–NS merger can be detected increases. Coincident survey transients (e.g. Scolnic et al. 2018), within the ET detection horizon $z \sim 0.5$, and GW merger signals will be key to characterizing the growing number of objects in the transient sky. The rate of transients at $z < 0.5$, with $m_{\rm r} \leq 26$, for our models is $(0.2 \lesssim R_{z<0.5} \lesssim 6.8) \times 10^{-3}\,{\rm deg}^{-2}\,{\rm yr}^{-1}$, and a mean rate $\langle R_{z<0.5} \rangle \sim 3.0 \times 10^{-3}\,{\rm deg}^{-2}\,{\rm yr}^{-1}$. For each model the rate is: (i) 4.5, (ii) 0.6, (iii) 0.2, (iv) 6.8, (v) 4.0, (vi) 2.4, and (vii) 5.1 where the units are $\times\, 10^{-3}\,{\rm deg}^{-2}\,{\rm yr}^{-1}$. These deep survey rates for a field of view 3300 deg^2 are: (i) 3.0(22.2), (ii) 0.5(20.4), (iii) 0.2(19.6), (iv) 12.6(114.6), (v) 3.3(24.2), (vi) 2.4(44.5), (vii) 2.4(23.7) yr^{-1}, where the number in brackets is without the redshift condition.

The rate of orphan afterglows from long GRBs is higher than that for short GRBs due to the difference in the occurrence rate of either transient. Long GRBs typically have jet half-opening angles $\theta_{\rm j} \sim 6^{\circ}$ (Ghirlanda et al. 2015). The peak afterglow for a highly inclined system at $i > \theta_{\rm j}$ decreases rapidly with increasing angle; for long-GRB jets associated with SNe, the peak flux rapidly falls below the peak of the accompanying SN[4] where the absolute magnitude is typically $M \sim -19$. If the majority of long-GRB jets are from core-collapse SNe, then the orphan afterglow will be hidden by the SN for systems inclined at $i \gtrsim 20^{\circ}$ away from the jet axis (Kathirgamaraju, Barniol Duran & Giannios 2016), this will reduce the number of detectable orphan afterglows from long GRBs, where it is assumed that all long GRBs have narrow homogeneous jets. Using the condition that an orphan afterglow from a long GRB must be inclined $i \leq 20^{\circ}$, the fraction of the total population could be lower than the predicted 50 yr^{-1}.

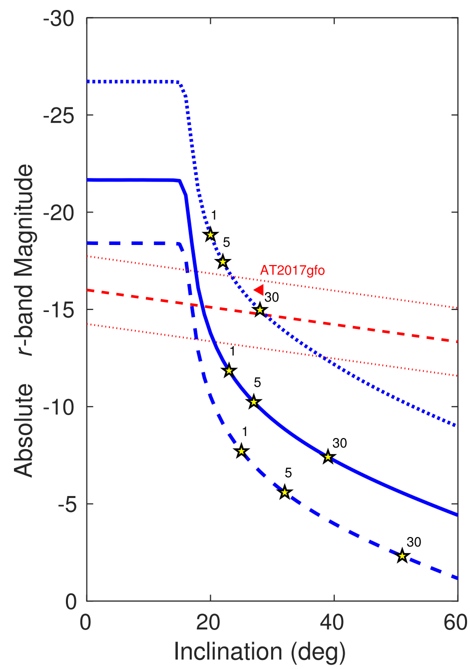

Figure 2. The peak afterglow in the *r*-band with the system inclination. The blue line indicates the peak observed *r*-band absolute magnitude at a given system inclination. The jet is a homogeneous jet with a half-opening angle of 16° and an energy $E_{\rm iso} = 5 \times 10^{48}$ erg for the dashed blue line, $E_{\rm iso} = 10^{50}$ erg for the solid blue line, and $E_{\rm iso} = 10^{52}$ erg for the dotted blue line. The yellow stars indicate the peak time after the merger in days at those points. The red lines indicate the expected peak macro-/kilo-nova *r*-band magnitude with inclination. The dotted red lines indicate the observed diversity of macro-/kilo-nova peak fluxes.

Fig. 2 shows how the absolute magnitude for an observer in the *r*-band changes with inclination for a homogeneous jet with $\theta_{\rm j} = 16^{\circ}$ and a range of isotropic equivalent energies $5 \times 10^{48} \leq E_{\rm iso} \leq 10^{52}$ erg. The peak *r*-band macro-/kilo-nova flux is shown as a red line, where the range is the observed diversity (Gompertz et al. 2017) which agrees with the predicted range for macro-/kilo-nova peak magnitudes in Tanaka & Hotokezaka (2013) and Barnes & Kasen (2013). For jets from mergers, the associated macro-/kilo-nova emission, although isotropic, is generally considered to be fainter for increasing observation angles (e.g. Tanaka et al. 2014; Tanaka 2016; Metzger 2017; Wollaeger et al. 2017). The macro-/kilo-nova decline with inclination shown in Fig. 2 assumes a linear trend from an 'on-axis' view to an edge-view, where the change in magnitude is that from Wollaeger et al. (2017). The macro-/kilo-nova associated with GW170817 is shown as a red triangle at an inclination of 28° (see for example: Abbott et al. 2017; Coulter et al. 2017; Drout et al. 2017; Evans et al. 2017; Metzger 2017; Murguia-Berthier et al. 2017; Pian et al. 2017; Smartt et al. 2017; Tanaka et al. 2017,2018; Tanvir et al. 2017, etc.). Macro-/kilo-nova will typically peak in the *r*-band $\lesssim$5 d after the merger for an observer at any inclination. However, the jet afterglow peak flux time is much later for an off-axis observer (days to months) than for an on-axis observer (minutes to hours). Where an orphan afterglow

[4] This depends on the *K*-corrected luminosity of the SN (Prentice et al. 2016). GRB afterglows are brighter over a broader spectrum than SNe due to the non-thermal nature of the emission, the off-axis GRB afterglow spectrum is increasingly shifted to lower frequencies as the observation angle increases, this effectively contributes to the reduction in the observed off-axis flux for an orphan afterglow at optical frequencies.

peaks $\lesssim$1 d or $\gtrsim$5 d, a survey telescope may have two opportunities to observe the merger, one from the afterglow and a second from the macro-/kilo-nova; the afterglow transient will typically fade much slower than that from a macro-/kilo-nova and will have a non-thermal spectrum. Thus, even if the transients have coincident peaks, the afterglow will fade more slowly than the macro-/kilo-nova. Additionally, due to the broad-band nature of the afterglow a radio transient should accompany the optical, possibly peaking at a later time depending on the inclination of the system.

The orphan afterglow population may be dominated by low-luminosity GRBs. Such low-luminosity GRBs form a distinct population (Wanderman & Piran 2010), where the rate is greater than that for long GRBs. The afterglow from low-luminosity GRBs is fainter than that for long GRBs (Barniol Duran et al. 2015), but the lower Lorentz factor of the ejecta means that any off-axis emission will have a reduced beaming effect. Where an orphan afterglow is brighter than the accompanying SNe, then low-luminosity GRB orphan afterglows may dominate the blind survey population.

The jets that produce long GRBs may exhibit the same structure or dynamical diversity as proposed for merger jets, the number of detectable orphan afterglows from long-GRB or collapsar jets will be higher than that predicted by assuming homogeneous structured jets. The increased rate of orphan transients from either collapsar jets or merger jets would indicate the presence of intrinsic jet structure or a dominant population of low-Γ jets. If long-GRB jets follow the latter, i.e. a dominant low-Γ population (Hascoët et al. 2014), the rate of orphan afterglows from collapsar jets would be higher by a similar fraction to that demonstrated here for merger jets with the LK16 model (iv). The light curve of an on-axis orphan afterglow will appear phenomenologically the same as a GRB afterglow, i.e. a power-law decay, $\propto t^{-1}$, with an observable break at late times. Whereas an off-axis orphan afterglow would decay with a steep, $\propto t^{<-2}$, decline with no jet-break.

We used a population of mergers that follow a lognormal time delay redshift distribution (Wanderman & Piran 2015). If NS/BH–NS mergers follow a power-law time delay distribution that peaks $z \sim 1.5$–2, then a higher fraction of the short GRB population would go undetected due to the large luminosity distance. The observation of a host for short GRB 111117A at $z = 2.211$ could challenge the lognormal time delay model, although this redshift is still within the lognormal limits, the probability is $\sim$2 orders of magnitude lower than for the peak at $z = 0.9$ (Selsing et al. 2017). Detectable orphan afterglows from a power-law time delay redshift distribution will follow the rates predicted here where $m_{\rm r} \lesssim 23$. A significant excess would exist at very faint magnitudes, $m_{\rm r}$ >26–28, where the population distribution peaks at a redshift $z \gtrsim 1.5$. The peak of the redshift distribution can be traced by the faint transients. For a discussion of a short-GRB population with such a distribution, see Sun et al. (2015) and Ghirlanda et al. (2016).

6 CONCLUSIONS

We have shown that the rate of orphan afterglows from merger (non-collapsar) short GRBs detectable by the LSST is $5 \lesssim R_{\rm OA} \lesssim 70\,{\rm yr}^{-1}$, where the rate is $\sim 7.3\,{\rm yr}^{-1}$ for a population of homogeneous jets with $\theta_{\rm j} = 16^\circ$. Where GRB afterglows are included, the rates become $16 \lesssim R_{\rm AG} \lesssim 76$ and $\sim 19\,{\rm yr}^{-1}$ for homogeneous jets with $\theta_{\rm j} = 16^\circ$. The ZTF detection rate for orphan afterglows from short GRBs is low $0.5 \lesssim R_{\rm OA} \lesssim 3.6$, the rate for afterglows with or without a *Swift*/BAT detectable GRB is $2 \lesssim R_{\rm AG} \lesssim 8\,{\rm yr}^{-1}$, and $\sim 4.2\,{\rm yr}^{-1}$ for a population of homogeneous jets with $\theta_{\rm j} = 16^\circ$.

For populations of jets narrower than $\theta_{\rm j} = 16^\circ$, the rate of orphan afterglows increases. For LSST, the orphan afterglow rate from a population of narrow short-GRB jets is $\sim 13.4\,{\rm yr}^{-1}$. This increase is due to the increased rate in the parent merger population due to the normalization required to produce the detectable all-sky *Swift*/BAT non-collapsar GRB rate.

If the population of jets that produce short GRBs is dominated by jets with a low-Γ, then the rate of orphan afterglows will increase significantly, $\sim 70\,{\rm yr}^{-1}$ for LSST and $\sim 3.6\,{\rm yr}^{-1}$ for ZTF. Where these jets result in fGRBs and are viewed within the jet half-opening angle, the light curve will appear phenomenologically the same as an on-axis GRB afterglow light curve.

If jets exhibit intrinsic structure, where the jet energetics extend beyond a homogeneous core to a defined edge, then the rate of orphan afterglows is greater than that for a homogeneous population; with the exception of the two-component jet structure when compared to the narrowest homogeneous jet population.

If LSST modifies the observation strategy from a fast survey to a deep-drilling field, then the obtainable sensitivity will increase. By focusing on a single field, the potential to detect the same transient with multiple observations increases and with this the ability to identify orphan afterglows. As shown in Fig. 1 and Table 1, the rate of detectable merger-jet transients increases significantly from a limiting magnitude of 24.5 to 26 for a population of narrow jets, a jet population dominated by low-Lorentz factors, or jets with intrinsic structure.

The structured or dynamical models tested here could equally be applied to collapsar or long-GRB jets. The observed rate of orphan afterglows from such jets would increase by a similar fraction for each case. Careful filtering of transients is required to successfully identify an orphan afterglow from either short- or long-GRB jets. Orphan afterglows fade rapidly and will rarely be above the detection threshold >1 d; single-point candidate identification and fast targeted follow-up will be required.

ACKNOWLEDGEMENTS

This research is supported by STFC grants . The authors thank the anonymous referee for helpful comments, and Samaya Nissanke and the participants of the Nordita ‘The Physics of Extreme Gravity Stars’ workshop and conference 2017 for useful discussions. GPL thanks Simon Prentice for helpful comments.

REFERENCES

Abbott B. P. et al., 2017, ApJ, 848, L12
Band D. L., 2006, ApJ, 644, 378
Barnes J., Kasen D., 2013, ApJ, 775, 18
Barnes J., Kasen D., Wu M.-R., Martínez-Pinedo G., 2016, ApJ, 829, 110
Barniol Duran R., Nakar E., Piran T., Sari R., 2015, MNRAS, 448, 417
Baumgartner W. H., Tueller J., Markwardt C. B., Skinner G. K., Barthelmy S., Mushotzky R. F., Evans P. A., Gehrels N., 2013, ApJS, 207, 19
Behroozi P. S., Ramirez-Ruiz E., Fryer C. L., 2014, ApJ, 792, 123
Bellm E., 2014, in Wozniak P. R., Graham M. J., Mahabal A. A., Seaman R. eds, The Third Hot-wiring the Transient Universe Workshop (HTU-III). Los Alamos National Laboratory, Santa Fe, New Mexico, p. 27
Bellm E., Kulkarni S., 2017, Nature Astron., 1, 0071
Berger E., 2014, ARA&A, 52, 43
Bloom J. S., Djorgovski S. G., Kulkarni S. R., Frail D. A., 1998, ApJ, 507, L25
Bogomazov A. I., Lipunov V. M., Tutukov A. V., 2007, Astron. Rep., 51, 308
Bromberg O., Nakar E., Piran T., Sari R., 2013, ApJ, 764, 179

Cenko S. B. et al., 2013, ApJ, 769, 130
Coulter D. A. et al., 2017, Science, 358, 1556
Coward D. M., Branchesi M., Howell E. J., Lasky P. D., Böer M., 2014, MNRAS, 445, 3575
D'Avanzo P. et al., 2014, MNRAS, 442, 2342
Dermer C. D., Chiang J., Mitman K. E., 2000, ApJ, 537, 785
Dionysopoulou K., Alic D., Rezzolla L., 2015, Phys. Rev. D, 92, 084064
Djorgovski S. G., Kulkarni S. R., Bloom J. S., Goodrich R., Frail D. A., Piro L., Palazzi E., 1998, ApJ, 508, L17
Drout M. R. et al., 2017, Science, 358, 1570
Eichler D., Livio M., Piran T., Schramm D. N., 1989, Nature, 340, 126
Evans P. A. et al., 2017, Science, 358, 1565
Fong W., Berger E., Margutti R., Zauderer B. A., 2015, ApJ, 815, 102
Fruchter A. S. et al., 2006, Nature, 441, 463
Ghirlanda G., Nava L., Ghisellini G., Celotti A., Firmani C., 2009, A&A, 496, 585
Ghirlanda G. et al., 2015, A&A, 578, A71
Ghirlanda G. et al., 2016, A&A, 594, A84
Goldstein A., Connaughton V., Briggs M. S., Burns E., 2016, ApJ, 818, 18
Gompertz B. P. et al., 2017, preprint (arXiv:1710.05442)
Gottlieb O., Nakar E., Piran T., 2018, MNRAS, 473, 576
Granot J., Panaitescu A., Kumar P., Woosley S. E., 2002, ApJ, 570, L61
Gruber D. et al., 2014, ApJS, 211, 12
Hascoët R., Beloborodov A. M., Daigne F., Mochkovitch R., 2014, ApJ, 782, 5
Hotokezaka K., Piran T., 2015, MNRAS, 450, 1430
Hotokezaka K., Nissanke S., Hallinan G., Lazio T. J. W., Nakar E., Piran T., 2016, ApJ, 831, 190
Huang Y. F., Dai Z. G., Lu T., 2002, MNRAS, 332, 735
Ioka K., Nakamura T., 2001, ApJ, 554, L163
Jin Z.-P. et al. 2017, preprint (arXiv:1708.07008)
Kathirgamaraju A., Barniol Duran R., Giannios D., 2016, MNRAS, 461, 1568
Kathirgamaraju A., Barniol Duran R., Giannios D., 2018, MNRAS, 473, L121
Kisaka S., Ioka K., Kashiyama K., Nakamura T., 2017, preprint (arXiv:1711.00243)
Kumar P., Panaitescu A., 2000, ApJ, 541, L51
Kyutoku K., Ioka K., Shibata M., 2014, MNRAS, 437, L6
Lamb G. P., Kobayashi S., 2016, ApJ, 829, 112
Lamb G. P., Kobayashi S., 2017, MNRAS, 472, 4953
Lazzati D., Deich A., Morsony B. J., Workman J. C., 2017, MNRAS, 471, 1652
Levan A., Crowther P., de Grijs R., Langer N., Xu D., Yoon S.-C., 2016, Space Sci. Rev., 202, 33
Li L.-X., Paczyński B., 1998, ApJ, 507, L59
LSST Science CollaborationAbell P. A., Allison J. et al., 2009, preprint (arXiv:0912.0201)
Margalit B., Piran T., 2015, MNRAS, 452, 3419
Metzger B. D., 2017, preprint (arXiv:1710.05931)
Metzger B. D., 2017, Living Rev. Relativ., 20, 3
Metzger B. D., Fernández R., 2014, MNRAS, 441, 3444
Metzger B. D., Zivancev C., 2016, MNRAS, 461, 4435
Mochkovitch R., Hernanz M., Isern J., Martin X., 1993, Nature, 361, 236
Murguia-Berthier A. et al., 2017, ApJ, 848, L34
Nakar E., 2007, Phys. Rep., 442, 166
Nakar E., Piran T., 2003, New A, 8, 141
Nakar E., Piran T., 2011, Nature, 478, 82
Nakar E., Piran T., 2017, ApJ, 834, 28
Narayan R., Paczynski B., Piran T., 1992, ApJ, 395, L83
Nissanke S., Kasliwal M., Georgieva A., 2013, ApJ, 767, 124
O'Shaughnessy R., Bellovary J. M., Brooks A., Shen S., Governato F., Christensen C. R., 2017, MNRAS, 464, 2831
Pian E. et al., 2017, Nature, 551, 67
Piran T., 1999, Phys. Rep., 314, 575
Piran T., Nakar E., Rosswog S., 2013, MNRAS, 430, 2121
Prentice S. J. et al., 2016, MNRAS, 458, 2973
Punturo M. et al., 2010, Class. Quantum Gravity, 27,194002
Rezzolla L., Giacomazzo B., Baiotti L., Granot J., Kouveliotou C., Aloy M. A. 2011, ApJ, 732, L6
Rhoads J. E., 2003, ApJ, 591, 1097
Rossi E., Lazzati D., Rees M. J., 2002, MNRAS, 332, 945
Sabatini S., Roberts S., Davies J., 2003, Ap&SS, 285, 97
Sari R., Piran T., Narayan R., 1998, ApJ, 497, L17
Sari R., Piran T., Halpern J. P., 1999, ApJ, 519, L17
Scolnic D. et al., 2018, ApJ, 852, L3
Selsing J. et al., 2017, preprint (arXiv:1707.01452)
Siellez K., Boer M., Gendre B., Regimbau T., 2016, preprint (arXiv:1606.03043)
Smartt S. J. et al., 2017, Nature, 551, 75
Sun H., Zhang B., Li Z., 2015, ApJ, 812, 33
Sun H., Zhang B., Gao H., 2017, ApJ, 835, 7
Tanaka M., 2016, Adv. Astron., 2016, 634197
Tanaka M., Hotokezaka K., 2013, ApJ, 775, 113
Tanaka M., Hotokezaka K., Kyutoku K., Wanajo S., Kiuchi K., Sekiguchi Y., Shibata M. 2014, ApJ, 780, 31
Tanaka M. et al., 2018, ApJ, 852, 109
Tanaka M. et al., 2017, PASJ, 69, 102
Tanvir N. R. et al., 2017, ApJ, 848, L27
Tsang D., Read J. S., Hinderer T., Piro A. L., Bondarescu R., 2012, Phys. Rev. Lett., 108, 011102
Tsutsui R., Yonetoku D., Nakamura T., Takahashi K., Morihara Y., 2013, MNRAS, 431, 1398
Wanderman D., Piran T., 2010, MNRAS, 406, 1944
Wanderman D., Piran T., 2015, MNRAS, 448, 3026
Wollaeger R. T. et al., 2017, preprint (arXiv:1705.07084)
Xiao D., Liu L.-D., Dai Z.-G., Wu X.-F., 2017, preprint (arXiv:1710.00275)
Yonetoku D., Murakami T., Nakamura T., Yamazaki R., Inoue A. K., Ioka K., 2004, ApJ, 609, 935
Zhang B., 2013, ApJ, 763, L22
Zhang G. Q., Wang F. Y., 2018, ApJ, 852, 1
Zhang F.-W., Shao L., Yan J.-Z., Wei D.-M., 2012, ApJ, 750, 88
Zou Y. C., Wu X. F., Dai Z. G., 2007, A&A, 461, 115

This paper has been typeset from a TEX/LATEX file prepared by the author.